Interface transport barriers in magnetized plasmas

Claudia Norscini, Thomas Cartier-Michaud, Guilhem Dif-Pradalier, Xavier Garbet, Philippe Ghendrih, Virginie Grandgirard, Yanick Sarazin

Interface transport barriers in magnetized plasmas

Claudia NORSCINI, Thomas CARTIER-MICHAUD, Guilhem DIF-PRADALIER, Xavier GARBET, Philippe GHENDRIH*, Virginie GRANDGIRARD, Yanick SARAZIN

CEA, IRFM, F-13108 Saint-Paul-lez-Durance, France.
* corresponding author

E-mail: philippe.ghendrih@cea.fr

Abstract. We address the formation of Interface Transport Barriers using a generic turbulent transport model, reduced to 2D, and used to investigate interchange turbulence in magnetized plasmas. The generation of a transport barrier at the edge-SOL plasma interface is governed by a zonation regime in the edge region with closed field lines. It is triggered by a gap in the turbulent spectrum between zero, the zonal flow wave vector, and the wave vector of the spectrum maximum. This gap is controlled by the energy injection wave vector of the interchange instability and the Rhine scale that bounds the inverse cascade. Increasing the magnitude of the turbulence drive at given gap reinforces the transport barrier. In the interface transport barrier regime, edge relaxation bursts of turbulence regenerate the zonal flows that are eroded by damping processes such as collisions. The duration of the quiescent phase between the quasi-periodic relaxation events is then governed by the ion collision frequency. Such interface transport barrier can play the role of a seed barrier prior to a full bifurcation to improved confinement.

Turbulence self-organization plays a major role in transport properties within stratified media in geophysics [1], astrophysics [2] as well as laboratory plasma dedicated to magnetic fusion research [3, 4, 5] . An outstanding mechanism is the transition from a fully turbulent to the so-called zonation regime [6], where large scale anisotropic flows, the zonal flows [7], appear to undergo condensation to a regular pattern [8]. Such transitions have been investigated in reduced 2D models of the Hasegawa-Mima type [9, 10]. We are interested here in such a transition in fusion plasmas where an interchange-like instability [11, 12], akin to the Rayleigh-Bénard instability [13, 14, 15], drives the turbulence. Of interest is the transition between two regions with different zonal flow damping capability such as observed at the periphery of magnetically confined plasmas between the edge region, where the magnetic surfaces are closed, and the SOL [14, 16] region where magnetic surfaces intersect wall components. We report the formation of a transport barrier localized at the interface, i.e. separatrix, between the edge where zonal flows are weakly damped and SOL where the plasma wall boundary conditions govern zonal flow damping. A zonal flow condensation is localized by the separatrix and a transport barrier develops with large gradients extending across the separatrix in the edge and SOL regions. Such a regime is different from that of the stair-cases [17, 18, 19] that are not localized radially and appear to meander with time. The simplified turbulence model that is used addresses

particle transport driven by a poloidally symmetric source localized in the edge region [16, 20]. This fixed location well within the separatrix enforces particle transport that has been repeatedly observed experimentally to be unfavorable for developing improved confinement scenarios in magnetically confined plasmas [5, 21]. However, we show here that an interface transport barrier can develop depending on spectral properties, namely the gap between the zonal flow and the wave vector of maximum energy injection governed by the instability, possibly shifted to lower wave vector by inverse cascade features. Large collisionality is shown to weaken the transport barrier by on-setting quasi periodic relaxations and thus increase the effective transport through the barrier region. On the overall, the interface barrier remains relatively weak even at lowest collisionality mostly because these relaxation events have not been observed to be completely quenched. It must therefore be regarded as a seed mechanism playing a role in the localization and subsequent bifurcation towards a full pedestal with significant confinement improvement [22].

The turbulent pattern generation is investigated with a 2D fluid model of the interchange instability [11, 12], akin to several instability mechanisms driving turbulence governed by a generic plasma cross field current, itself driven by magnetic field inhomogeneity and consequent vertical drift current. The model is simplified to only retain the key features required for generating the interface transport barriers. It stands for particle and charge conservation equations in an isothermal plasma in the cold ion limit:

$$\partial_t n + [\phi, n] - D_\perp \Delta_\perp n = S - \Gamma \tag{1a}$$

$$\partial_t W + [\phi, W] - \nu_\perp \Delta_\perp W + \ g\partial_y n = J \tag{1b}$$

where n is the particle density and W the vorticity, $W = \Delta_\perp \Phi$. The time and space are normalized by the inverse of the cyclotron frequency and the Larmor radius respectively. Space is reduced to 2D transverse to the magnetic field assuming symmetry along the magnetic field. The y coordinate is typically an angle, the poloidal angle for magnetic confinement, the x coordinate in the radial direction that extends from the source S, localized in the edge, to the sink Γ in the SOL. The separatrix is defined at a given x_{Sep} radial position. Constraints due to the physics along the magnetic field govern volumetric loss terms: the parallel divergence of the electric current J and the particle sink Γ, the latter being specific of the SOL region. Convective turbulent transport $[\Phi, f] = \partial_x(f v_x) + \partial_y(f v_y)$ with electric drift velocity $v_x = -\partial_y \Phi$ and $v_y = \partial_x \Phi$ competes with weak diffusive transport with coefficient D for the particles and $\nu_\perp$ for the vorticity. The model is similar to the Rayleigh Bénard model [13, 14, 15], replacing the density n by the fluid thermal energy variation Θ [13] and the g-term, which governs the plasma interchange instability, by the buoyancy force. The electric potential is ϕ and W is related to the polarization charge. For standard fluids ϕ is the stream function and W the vorticity [13]. A pseudo-spectral code is used for the numerical simulations with state of the art verification by PoPe [23]. The high accuracy of the computation of the derivatives ensures that the small diffusive processes included in the evolution equations are not overwhelmed by spurious numerical diffusion.

The change in field line properties at the separatrix is taken into account by a mask function $\chi(x)$, $\chi(x > x_{Sep}) = 0$ and $\chi(x \leq x_{Sep}) = 1$ such that $J = \sigma_\phi(\phi - \chi(x) \langle \phi \rangle_y)$,where σ_ϕ is the normalized conductivity and $\langle f \rangle_y$ is the $y-$average

of f, similarly $\Gamma = (1-\chi(x))\sigma_n n$ where σ_n is the particle lifetime in the SOL. The edge and SOL difference is twofold. First the particle loss is localized in the SOL region. This has rather little effect on the turbulence but organizes the overall stratification of the system in the x direction. Second, the change in J modifies the evolution equation for the zonal flow $V_z = \partial_x \langle\phi\rangle_y$. The latter is governed by a balance between the non linear Reynolds stress source, and the loss terms: viscous damping at small scales, sink term $\langle J\rangle_y$ at large scales. The edge constraint $\langle J\rangle_y = 0$ favors large scale zonal flow structures. Conversely, in the SOL, the current loss $\langle J\rangle_y = \sigma_\phi \langle\phi\rangle_y$, here linearized for simplicity, damps these zonal flow structures. These specific loss terms are discussed in Appendix A both in terms of the underlying physics and regarding the effect on the instabilities determined by the dispersion relation.

In the strong zonation regime, exemplified in fusion plasmas by the so-called Dimits' shift [24, 25], the plasma appears to remain close to marginality. The linear analysis of the near marginal growth rate, for a prescribed and constant density gradient length $1/L_n$ and for eigen functions given by Fourier modes, is then:

$$\gamma_m = \frac{(\nu_\perp \sigma_\phi)^{1/2}}{L(K)} \left(\frac{L_R}{L_n} \frac{k_y^2}{k^2} - \frac{1}{S_c} \left(K^4 + 1\right) \right) \tag{2a}$$

$$L_R = \frac{g}{\nu_\perp \sigma_\phi} \quad ; \quad L(K) = (1 + 1/S_c)K^2 + 1/K^2 \tag{2b}$$

where $K = k/\bar{k}$, $\bar{k}^4 = \sigma_\phi/\nu_\perp$ and $S_c = \nu_\perp/D$ is the Schmidt number. This expression yields three key aspects of the near marginal regime, the order of magnitude of γ_m, $(\nu_\perp\sigma_\phi)^{1/2}$, the threshold such that L_R/L_n must exceed a given function of k_x and k_y, and a localization function $L(K)$ that favors $K = (1 + 1/S_c)^{-1/4}$ as most unstable mode. The latter effect is governed by the balance between the homogeneous damping rates, that at small scale $\approx \nu_\perp k^2$ due to diffusion, and that at large scale $\approx \sigma_\phi/k^2$ due to parallel currents. These loss terms govern dissipation for large and small wave vectors. They prevent energy accumulation in these spectral regions irrespective of the direction of the energy cascade. It is to be underlined that in the SOL, $\chi(x > x_{Sep}) = 0$, the large scale damping also applies to the zonal flows, which is not the case in the edge, $\chi(x < x_{Sep}) = 1$, as prescribed for adiabatic electrons. Finally, the drive for the interchange instability is proportional to k_y^2/k^2, and favors therefore modes with smallest values of k_x, excluding $k_x = 0$ to allow for global momentum conservation by the zonal flow radial structure.

SOL-transport with the present model is comparable to that previously reported when only the SOL region was addressed [16, 26]. It is characterized by avalanche transport, hence ballistic propagation of fronts and holes [16, 27, 26], the so-called 'blobs' [28] routinely observed in experiments [29, 30]. Density and potential fluctuations are large [16, 26] but the mean value weakly departs from the equilibrium value, namely the plasma floating potential set at zero for convenience in this isothermal case. Conversely, transport in the edge region appears to depend significantly on the zonal flows. These generate transport barriers [5, 7], where the transverse turbulent avalanches are damped and therefore where the remnant diffusive transport governs a larger fraction of the particle outflux [31]. The time averaged profiles then exhibit an enhanced gradient region, the so-called pedestal. At the edge and SOL interface this pedestal is readily observed, as shown on fig.1-a. Three different average density profiles are compared on fig.1-a where only the position of the separatrix x_{Sep} is modified in the simulations, i.e. $x_{Sep} = 0.6\ x_a$ (continuous line),

$x_{Sep} = 0.8\ x_a$ (dashed line) and $x_{Sep} = x_a$, dash-dot line). Three key features are highlighted by these results: the density e-folding length in the SOL is unchanged, the pedestal region with large density gradient at the separatrix extends both in the edge and SOL regions and the density profile exhibits corrugations, enhanced gradients at other locations, that yields a staircase-like profile [17, 18]. In order to quantify the

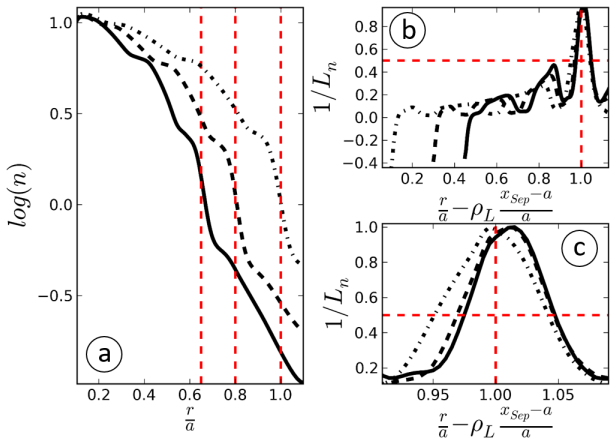

Figure 1: (a) Density pedestal for different positions of the separatrix (see text), (b) density gradient profiles with radial shift, (c) zoom on the pedestal region

extent of the pedestal in the two regions, we shift the profiles to the same separatrix position and compare the density gradient profiles $1/L_n = -\partial_x n\ /\ n$, fig.1-b. The strong density drop observed in the pedestal leads to a marked peak in the $1/L_n$ profile localized at the separatrix. The pedestal extends into both the edge and SOL regions. Its radial width is observed to range between 5 % and 10 % of the size of the simulation domain, of the same order of magnitude as the SOL width fig.1-c. Regions with large zonal flows shear appear to be correlated with the corrugation of the profiles, see fig.2-a & b. They are characterized by a stopping capability of most of the avalanches both overdense from uphill and holes from downhill [31, 32].
The plasma evolution in the edge is characterized by a slow reorganization of the zonal flow pattern as readily observed on the contour plot of the zonal flow shear superimposed on the 2D plot of $1/L_n$, fig.2-a. Two features are outstanding, the evolution towards a dipolar structure of $1/L_n$ in the edge region and conversely the structure of the maximum value at the separatrix that weakly evolves. When a statistical steady state is reached, one can average the profiles over time, fig.2-b and fig.2-d. As readily expected, one can see that the total flux $\Gamma_{tot} = \Gamma_{turb} + \Gamma_{diff}$ is radially constant in the edge and decays in the SOL. In the edge, the turbulent contribution Γ_{turb} exhibits well defined minima, and consequently large values of the diffusive flux Γ_{diff}, at locations where $1/L_n$ as well as the magnitude of the zonal flow shear are large. Narrow regions with strong turbulent transport are localized in the vicinity of the layers with zero shear of the zonal flows.

To identify the transport barriers, one defines the ratio between the y-averaged particle fluxes $R_b = \Gamma_{turb}/\Gamma_{tot}$ [31]. R_b varies between 0 and 1 in steady state and is a measure of the effectiveness of the barrier in reducing turbulent transport. One readily

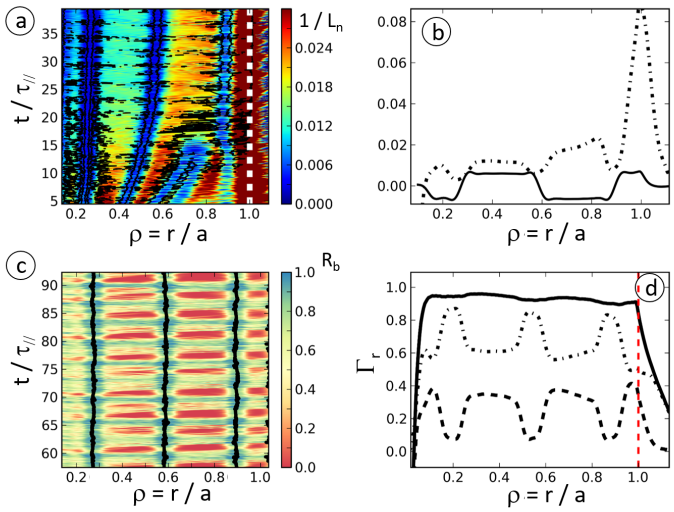

Figure 2: (a) $E \times B$ shear (contour) and $1/L_n$ (colored) in function of time and radius, separatrix location white vertical dashed line,(b) the time and y-averaged shear (plain) and $1/L_n$ (dash-dot), (c) parameter R_b used to determine the transport barriers, (d) total flux (plain), turbulent flux (dash-dot) and diffusive flux (dash) in the radial direction, separatrix location red vertical dashed line.

observes on fig.2-c that R_b changes in time and space (x-direction). In space, one recovers the dipolar structure with four transport barrier regions, the pedestal at the separatrix that is relatively narrow, two broad barriers in the edge and finally a small transport barrier towards the source region that is strongly linked to the boundary conditions of the model. In time, one can observe quasi-periodic relaxation events. These are characterized by strong turbulent transport across all the barriers. While these events are globally quasi-periodic, the detailed time evolution is quite specific of each event made of consecutive avalanches that do not extend throughout the edge region. These events also exhibit a marked correlation with the large transport bursts in the SOL region, see fig.3. In this turbulent transport regime, the pattern of the avalanches is quite complex and driven by several mechanisms, the source, the bouncing between the staircases [32, 33, 19], diffusive burn through the barriers and corrugations [31], as well as the wake of previous transport events that determine a pre-existing pattern of the electric potential [19]. As can be observed on the time traces, the edge region exhibits a sawtooth evolution pattern, corresponding to particle storage and subsequent relaxation by the interface transport barrier, while the SOL region exhibits a pulse-like variation, since the SOL acts as the sink for the particles released at each relaxation event, fig.3.

The generation of a pedestal, associated in this model to a corrugation structure in the edge region, is observed for values of the control parameters that are close to those yielding marginal interchange instability. However turbulent transport and zonation clearly indicate that non-linear features govern the evolution. The interplay between zonal and turbulent modes can be addressed in the modulational instability framework [34] with three mode coupling [7], $\phi_z(\kappa, 0)$, $\phi_s(0, k_y)$, $\phi_t(\kappa, -k_y)$, respectively the zonal flow (Z), a streamer (S) and a turbulent mode (t) [20]. In terms of wave vectors in

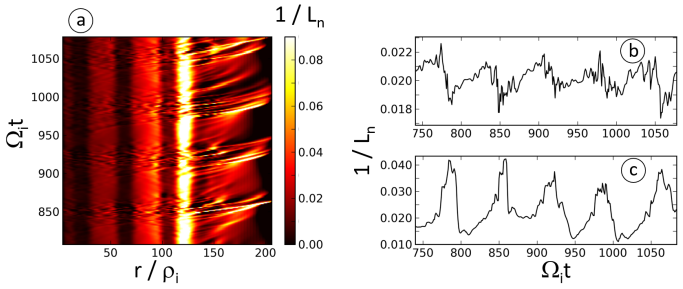

Figure 3: (a) $1/L_n$ evolution in time and radial direction, separatrix localized at $r = 120\rho_i$, with different SOL and edge transport patterns, time trace of $1/L_n$ at given radial positions in the edge (b), and SOL (c).

the x and y directions, both the zonal flow and the streamer are strongly asymmetric while the turbulent mode is more symmetric. Removing the interchange instability by setting $g = 0$, we can address analytically the dispersion relation in two limit cases (1) Z-flow generation with growth rate γ_1, given a finite amplitude of the streamer mode Φ_s as reference equilibrium and two coupled perturbation modes ϕ_z, ϕ_t, conversely, (2) a finite zonal saturation with mode amplitude Φ_z and two growing perturbation modes with amplitude ϕ_s, ϕ_t and growth rate γ_2. The dispersion relations for cases (1) and (2) are:

$$(\gamma_1 + \gamma_z)(\gamma_1 + \gamma_t) = \quad V_t k_y^2 \kappa^2 |\Phi_s|^2 \tag{3a}$$

$$(\gamma_2 + \gamma_t)(\gamma_2 + \gamma_s) = -V_t k_y^2 \kappa^2 |\Phi_z|^2 \tag{3b}$$

where $\gamma_z = \nu_\perp \kappa^2$, $\gamma_s = \nu_\perp k_y^2 + \sigma_\phi / k_y^2$ and $\gamma_t = \nu_\perp k^2 + \sigma_\phi / k^2$, $k^2 = \kappa^2 + k_y^2$. The coupling term is $V_t = \left(k_y^2 - \kappa^2\right)/k^2$. A symmetric necessary condition for positive growth rates of these two particular cases of Kelvin-Helmholtz instability [20] is obtained: in case (1) Eq.(3a) $k_y^2 > \kappa^2$, and in case (2) Eq.(3b) $k_y^2 < \kappa^2$.

Considering the turbulence spectrum in k_y, we split the mode domain in three regions: the zonal flow (Z) $k_y = 0$, the Big (B) $|k_y| < |\kappa|$ and Small (S) turbulent structures $|k_y| > |\kappa|$. Region S is the source of zonal flows while region B acts as a sink and energy loss via the large scale damping term proportional to σ_ϕ. Provided $\kappa \neq 0$, the viscosity term is a generic version of damping at large scales that includes ion collisions, and that actually controls the linear damping of zonal flows [35]. The existence of the B-mode region is essential for the transition from a turbulent regime to the zonation regime characterized by the development of a non homogeneous spectrum, $|k_y| < |k_x| \approx \kappa$. Furthermore, the shearing capability of the $k_x = \kappa$ zonal flow is small for the B-modes since $|k_y| < |\kappa|$. For $g \neq 0$, the energy injection in the spectrum is governed by the interchange instability at $k_y \approx \bar{k}$ and the inverse cascade [36] is controlled by the Rhine scale L_R, eq.(2). The development of the B-mode gap between the turbulence modes and zonal flows is thus constrained by $\kappa \approx \kappa_R \gg 1$, where $\kappa_R = \min(\bar{k}, 1/L_R)$.

The spectrum of the electric potential in simulations in the zonation regime, fig.4-a, is characterized by a gap between S and Z modes, hence with weak B-mode turbulence. The S-region then transfers energy via non linear coupling towards the

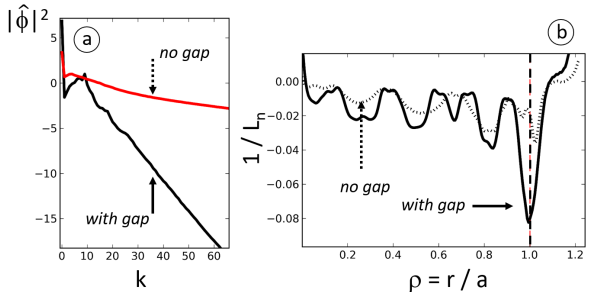

Figure 4: (a) Electric potential spectrum, turbulent regime labeled "no gap" and zonation regime with interface transport barrier labeled "with gap". (b) density gradient profile: zonation regime, plain line, labeled "with gap"), and turbulent regime, dashed line labeled "no gap", the separatrix is indicated by the vertical dashed line at $\rho = r/a = 1$.

Z-flows, which tends to store the energy and quench turbulent transport dominated by the S-modes. The Z-mode decays gradually due to viscous damping while the Interface Transport Barrier gradient builds-up until a new relaxation event is triggered. The onset of the latter is mostly governed by the zonal flow weakening. However, at lowest collisionality, when the relaxation frequency is small enough that large gradient build-up, the gradient increase can combine to the zonal flow decay and drive the onset of a burst of turbulent transport. The burst of S-mode turbulence leads to the gradient relaxation as well as Z-flows regeneration. Conversely, when the gap between the S and Z spectral regions is reduced, hence increasing the B-mode amplitude, the B-mode turbulent activity is less affected by Z-flow shearing and the Z-mode energy is transferred back to the turbulent modes, both the B and S modes according to the mechanism yielding the Kelvin-Helmholtz dispersion relation Eq.(3b). In that regime, the relaxation events cannot be isolated from the steady state transport activity and the pedestal is smeared-out, fig.4-b. The fluctuations spectra that characterize these two regimes present a strong similarity with the experimental observation achieved during the claimed L-H transition on the stellarator H-1 [37].
The dynamics of this transition between pedestal (High confinement) and no-pedestal (Low-confinement) behavior, is captured by the following 0-D predator-prey model [7]. The model couples the gradients ∇n and the Z, S and B modes. The gradient ∇n is governed by a balance between the source P and transport, both turbulent $T = B + S$ and collisional T^*. The growth rates for S and B modes are γ_s and γ_b respectively and exhibit a threshold in the gradient, ∇n^*. Non-linear saturation of these modes are used, proportional to α_s and α_b. The control parameter of the Z-flow generation by S is β. The B-modes act as a saturation term on this energy exchange via the $1/T$

dependence. The Z-flow sink is proportional to the viscosity ν.

$$\frac{\partial_t \nabla n}{\nabla n} = \frac{P}{\nabla n} - (T + T^*) \qquad ; \qquad T = B + S \tag{4a}$$

$$\frac{\partial_t Z}{Z} = \beta \frac{S}{T} - \nu \tag{4b}$$

$$\frac{\partial_t S}{S} = \gamma_s (\nabla n - \nabla n^*)(1 - \alpha_s S) - \beta \frac{Z}{T} \tag{4c}$$

$$\frac{\partial_t B}{B} = \gamma_b (\nabla n - \nabla n^*)(1 - \alpha_b B) \tag{4d}$$

This system is similar to predator-prey models introduced to describe plasma turbulent transport with reduced models [31, 38, 39]. One difference however is that the predating of turbulence by zonal flow shearing takes a form that is reminiscent of a κ-ε model [40, 41]. The field ε that acts as a predator of the turbulence energy, typically the S-modes is then defined as $\varepsilon = \beta(S/T)Z$. The energy transfer mechanism towards the energy sink is therefore governed by the zonal flows with a particular efficiency that depends on the ratio S/T, namely the transfer is inhibited whenever $B \gtrsim S$. When changing variable Z to ε, one finds the standard local evolution of the κ-ε model assuming that B stands for κ.

$$\partial_t S = \gamma_s (\nabla n - \nabla n^*)(1 - \alpha_s S) S - \varepsilon \tag{5a}$$

$$\partial_t \varepsilon = \gamma_\varepsilon \varepsilon - \frac{\varepsilon^2}{S}\left(1 - \frac{S}{T}\right) \tag{5b}$$

The growth rate for ε is a complicated expression, essentially determined by the frequency β and the growth rate of B as well as an inhibiting effect due to the specific linear zonal flow damping proportional to ν. The saturation term in the ε model is reminiscent of that used in neutral fluid turbulence [40], but with an efficiency that depends on the ratio B/T so that for $B \simeq T$ this non-linear saturation is effective while it is impeded when B decreases with respect to S. In the latter case, a case with a gap since $B \ll S$, the stabilizing role of ε is enhanced. The limit cycles of the Z-T interplay in simulations and the 0-D model are compared in the $Z - T$ plane, fig.5-a. Z and T are readily determined by eq.(4) for the 0-D model. For the simulation output of interchange turbulence, we define $Z_i = FT(V_z)$ and $T_i^2 = FT(R)$ as the 2D Fourier mode energy FT of the zonal flow velocity V_z and Reynolds stress R respectively. The different positions of the cycles in the Z-T plane are determined by the control parameters: blue trace for a reference case. Increasing the curvature term g leads to the yellow trace, while decreasing σ_ϕ leads to the green trace, fig.5-b. Increasing g in the simulation leads to an increase of both turbulence and zonal flow energies, the latter more strongly, so that of Z_i/T_i increases. A comparable behavior is obtained by increasing γ_s and γ_b, namely the growth rate of the interchange instability -governed by g- fig.5-b. Decreasing σ governs a decrease of both $\bar{k}$ and $1/L_R$ so that the spectrum maximum shifts towards the low k_y values, reducing the Z-S gap. The turbulence amplitude is then increased as well as the ratio between B and S modes. Consistently, this behavior is recovered in the 0-D model by reducing α_s and α_b, the non-linear turbulence saturation, as well as the critical gradient ∇n^*.

The occurrence of an interface localized where some mechanisms at play in the vorticity evolution change rapidly is shown to drive a transport barrier in some parameter regimes. This barrier is pinned at the interface and extends across the interface.

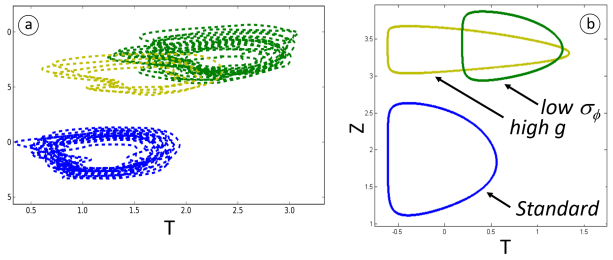

Figure 5: Limit cycles: (a) 2D simulation,(b) 0D model

In fusion plasmas a possible drive for such a behavior is the change in zonal flows damping across the separatrix between open and closed field lines. Similar changes could also take place across the separatrix of MHD modes. Although this mechanism seems ubiquitous in driving weak transport barriers whenever an interface exists, it does not exhibit all the key features that govern H-mode transport barriers. It could however, be a mechanism for weak transport barrier formation at the separatrix in X-point divertor configurations as well as at the last closed magnetic surfaces in limiter configurations. This would be a seed mechanism localizing the H-mode transport barrier when other mechanisms reinforce the transition to large transport barriers. Conversely, in simulations with a different implementation, or different resolution, between two simulation domains, and in particular at the separatrix, it can also lead to spuriously large interface barriers. Finally in conjunction with MHD island mode structure it could be a seed mechanism explaining the correlation, although non-systematic, between radial localization of Internal Transport Barrier and rational safety factors [42, 43]. Rapid variation of the zonal flow damping rate is also found to be a key mechanism of barrier formation when neoclassical dependencies are accounted for [44]. It can also play a role in the barrier behavior reported in [45] as well as in a 3D global simulation with realistic divertor configuration [46]. Recent results with penalized boundary conditions [47, 48] and gyrokinetic turbulence are characterized by a transport barrier at the interface between the magnetic surfaces with penalized conditions and that without [48, 49]. One also finds in gyrokinetic simulations that collisionless regimes with strong zonation yield stiff corrugation patterns such that turbulent transport quenching can drive a divergence of the profiles in these flux driven simulations [50].

We show here that the generic mechanism generating such an interface transport barrier is the ability to open a gap between the turbulent mode with largest amplitude and the zonal flows. When such a gap occurs the intermediate modes are depleted by zonal flow shearing and energy tends to condensate on the zonal flows, hence sustaining the transport barrier. However, when the gap is reduced, the intermediate modes provide a mechanism for depleting the zonal flows, thus reducing the turbulence quenching capability. This mechanism is similar to that observed experimentally on the stellarator H-1 [37]. One also finds that such a transport barrier is prone to cyclic relaxation events governed by the erosion of the zonal flows, in particular by collisions. Low collisionality would then govern a lowered frequency of the turbulent bursts and the possibility to develop enhanced gradients at the interface. The physics that control the gap are governed by the mode of the energy injection into the spectrum combined

to inverse cascade effects that tend to shift the spectrum maximum towards the low mode numbers. It can be shown that stepping to finite ion temperature inhibits the inverse cascade. Furthermore, higher edge plasma temperatures increase the parallel conductivity σ_ϕ and should therefore drive the most unstable mode $\overline{k}^4 = \sigma_\phi/\nu_\perp$ to higher values. Finally, the increase of the ion temperature will reduce the zonal flow collisional damping rate. This discussion indicates that although the role of the plasma temperature in the edge, and more specifically the ion temperature and therefore of the energy flux on the ion heat channel, is not addressed in the model, it appears to be a means to control the spectral gap between the zonal flows and the wave vector of the spectrum maximum. Experimental evidence would then support a mechanism that controls the spectral gap and drives the onset of seed transport barriers localized at the interface where rapid variation in space of zonal flow damping takes place.

Acknowledgements

This work has also been inspired by numerous discussions with Prof. P. Diamond during the Festival de Théorie, a meeting that enables in depth scientific exchange. The results presented have been obtained in the framework or Claudia Norscini's PhD. This work was carried out within the framework of the EUROfusion Consortium and has received funding from the Euratom research and training programme 2014 – 2018 and 2019 - 2020 under grant agreement No 633053. The views and opinions expressed herein do not necessarily reflect those of the European Commission.

Appendix A. Specific sink terms and the dispersion relation

The model (1) is a simplification of the model used in [36, 16, 14] to investigate SOL turbulence driven by the interchange instability [11, 12]. Via an integration along the field lines it depends on the electron particle flux as determined by the sheath conditions $\Gamma_n = nc_s \exp(\Lambda - \phi)$ where c_s is the sound velocity and $n\exp(\Lambda - \phi)$ the electron density variation in the adiabatic limit for parallel momentum balance. In the isothermal case used here Λ is related to the floating potential. We consider here that Λ is a constant so that it can be set to zero when changing the reference electric potential. The current loss J through the plasma sheath is then determined by the ion current, the so called ion saturation current enc_s, and the electron current $e\Gamma_n$ so that $j = enc_s(1 - \exp(\Lambda - \phi))$. The adiabatic electron response in the parallel direction drives a highly non-linear dependence that is of interest when addressing a precise description of these losses [14] but that can be linearized to capture the key features of the instabilities, therefore $\Gamma_n \approx c_s(n - n_0\phi)$ and $j \approx en_0c_s\phi$.
In the edge, following the Hasegawa-Wakatani seminal model [51] the current is proportional to the electron particle flux so that $\Gamma_n = (\sigma T_e/e^2)\nabla_\parallel(n/n_0 - \phi)$ where σ is the electric conductivity. The characteristic loss terms in both (1a) and (1b) are then of the form $C(n - \phi)$ where $C \propto k_\parallel^2$. The dependence in the parallel wave vector $k_\parallel$ stems from the fact that the current j is proportional to the parallel gradient of the electron plasma pressure and of the electric potential and that the divergence of these fluxes determine the local loss terms due to the parallel dynamics, hence a dependence in $k_\parallel^2$. Two important remarks must then be made. First, for the flux surface average, the y-average in the 2D case of model (1), one has $k_\parallel = 0$ so that these loss terms vanish. Second, in the asymptotic limit $C \to +\infty$, hence when the collisional friction in the electron mechanical balance become negligible, one recovers the adiabatic limit for the fluctuations $n = \phi$. The edge loss terms introduced in the Hasegawa-Wakatani model are thus suitable for fluctuations but cannot be extended to include the complete field as considered in the global framework of our model (1). This point is of particular importance for the density field since the parallel loss term in the sheath is proportional to $n = \langle n\rangle + \widetilde{n}$ (1a) while $n - \langle n\rangle$ is implicitly considered in the Hasegawa-Wakatani term $C(n - \phi)$. The same difference holds for the electric potential ϕ.
Let us now address the dispersion relation determined by the linearized particle and charge balance equations in Fourier space for the Fourier mode of the density $\widehat{n}$ and of the potential $\widehat{\phi}$ with wave vector k_x in the x-direction and k_y in the y-direction and $k^2 = k_x^2 + k_y^2$.

$$\partial_t\widehat{n} + \frac{ik_y}{L_n}\widehat{\phi} + D_\perp k^2\widehat{n} = -G_n\widehat{n} - G_\phi\widehat{\phi} \tag{A.1a}$$

$$\partial_t\widehat{\phi} - \frac{ik_yg}{k^2}\widehat{n} + \nu_\perp k^2\widehat{\phi} = -\frac{J_n}{k^2}\widehat{n} - \frac{J_\phi}{k^2}\widehat{\phi} \tag{A.1b}$$

In this expression the density gradient length $1/L_n = -\partial_x n/n$ is chosen to be constant and is a measure of the departure from equilibrium. Here, $G_n\widehat{n} + G_\phi\widehat{\phi}$ is the linearized and Fourier transformed expression of Γ and $(-J_n/k^2)\widehat{n} + (-J_\phi/k^2)\widehat{\phi}$ is the linearized and Fourier transformed expression of J divided by $-k^2$. The growth rate γ for the non-trivial solution of the coupled set of linear equations (A.1) is determined by the vanishing determinant condition, which then yields a generic second order equation in

γ of the form:

$$\gamma^2 + 2A\gamma + A_n A_\phi - B_n B_\phi = 0 \tag{A.2a}$$

with $A = (A_n + A_\phi)/2$ and A_n, A_ϕ are the damping rates for the density and electric potential respectively and where B_n and B_ϕ are the coupling terms between the two equations: $A_n = D_\perp k^2 + G_n$, $A_\phi = \nu_\perp k^2 + J_\phi/k^2$, $B_n = ik_y/L_n + G_\phi$, $B_\phi = -ik_y g/k^2 + J_n/k^2$. The coefficients A_n and A_ϕ are damping rates standing for the competing diffusive transport that inhibits the convective transport, G_n that stands for parallel particle loss, and J_ϕ that is a parallel current that will tend to compensate the cross field current due to the vertical drifts and taken into account via the contribution proportional to g. The coupling terms are complex coefficients such that the two imaginary parts are the key terms that drive the interchange instability while the two real parts are the coefficient that drive the drift wave instability. A general case will therefore couple these two linear instability mechanisms. On general grounds, such a competition is of course quite interesting, however at the cost of making the study of the non-linear stage of the flux-driven system more difficult to analyze.

We have decided to only retain the interchange instability by setting $G_\phi = 0$ and $J_n = 0$. As discussed above, the latter assumption regarding the linearized loss terms $J_n = 0$ appears to hold in the SOL where the ion current if of the same order as the electron current. Furthermore, in the edge the parallel particle transport is restricted to the fluctuating par of n. Conversely, setting $G_\phi = 0$ has little justification but that of simplifying the problem at hand. Changing notations to $\sigma_\phi = J_\phi$ and $\sigma_n = G_n$ allows one to recover (1). In the edge, taken into account by the mask function $\chi(x)$, both σ_n and σ_ϕ vanish for $k_\parallel = 0$ so that the loss terms are only governed by the fluctuations. We enforce this property for the current losses since this effect plays a strong role in the regulation of the zonal flows ($k_y = 0$). For the particle losses in the edge, we simplify the problem by ignoring this loss term and σ_n is set to zero in the edge by the mask function. The loss terms simplified in this way provide a setting of the system with minimum difference between the edge and SOL conditions, therefore a simplified interface where in fact a single key mechanism changes, and such that the analysis is not too involved by retaining a single primary linear instability.

One then finds $B_n B_\phi = (g/L_n)k_y^2/k^2$, hence $B_n B_\phi \in \mathbb{R}^+$ so that the two roots for the growth rate are real and an instability threshold, one positive root, is obtained when $B_n B_\phi \geq A_n A_\phi$, namely when the interchange instability drive $(g/L_n)k_y^2/k^2$ is larger than the damping processes $(D_\perp k^2 + \sigma_n)(\nu_\perp k^2 + \sigma_\phi/k^2)$.

$$\gamma = A\Big(-1 + \sqrt{1 + \frac{B_n B_\phi - A_n A_\phi}{A^2}}\Big) \tag{A.2b}$$

Near marginality, when $B_n B_\phi - A_n A_\phi \ll A$ and $B_n B_\phi \geq A_n A_\phi$, the expansion of (A.2b) then yields:

$$\gamma \approx \frac{B_n B_\phi - A_n A_\phi}{2A} \tag{A.2c}$$

One can then readily step to (2) computed for edge conditions by setting $\sigma_n = 0$.

Appendix B. Dispersion relation for three wave coupling

The complete calculation of the modulational instability including interchange leads to a relatively complicated dispersion equation [20]. For the sake of simplicity we analyze here some of the key properties obtained by setting $g = 0$ in (1b).

$$\partial_t W + [\phi, W] + \mathcal{A}_\phi W = 0 \tag{B.1}$$

Here $\mathcal{A}_\phi W$ stands for the linear damping part of the vorticity equation, thus according to (1b) $\mathcal{A}_\phi W = -\nu_\perp \Delta_\perp W - J$. We are interested in the Fourier mode analysis in the 2D space transverse to the unit vector $\boldsymbol{z}$ (in the third dimension). The quadratic nonlinear term the yields generically a convolution operator. Restricting the number of modes to three coupled wave vectors, $\boldsymbol{k}_1$, $\boldsymbol{k}_2$, $\boldsymbol{k}_3$ such that $\boldsymbol{k}_1 = \boldsymbol{k}_2 + \boldsymbol{k}_3$ and with amplitude $\widehat{\phi}_1$, $\widehat{\phi}_2$, $\widehat{\phi}_3$. Assuming the amplitude $\widehat{\phi}_3$ to be fixed we then obtain the following set of coupled equation for the mode amplitudes $\widehat{\phi}_1$ and $\widehat{\phi}_2$.

$$\partial_t \widehat{\phi}_1 - \frac{k_3^2 - k_2^2}{k_1^2}\Big(\boldsymbol{z}\cdot\big(\boldsymbol{k}_2 \times \boldsymbol{k}_3\big)\Big)\widehat{\phi}_2\widehat{\phi}_3 + A_\phi(\boldsymbol{k}_1)\widehat{\phi}_1 = 0 \tag{B.2a}$$

$$\partial_t \widehat{\phi}_2 - \frac{k_3^2 - k_1^2}{k_2^2}\Big(\boldsymbol{z}\cdot\big(\boldsymbol{k}_3 \times \boldsymbol{k}_1\big)\Big)\widehat{\phi}_1\widehat{\phi}_3^* + A_\phi(\boldsymbol{k}_2)\widehat{\phi}_2 = 0 \tag{B.2b}$$

This general system (B.2) can first be simplified with the particular choice $\boldsymbol{k}_1 = \boldsymbol{k}_t = (\kappa, k_y)$, $\boldsymbol{k}_2 = \boldsymbol{k}_s = (0, k_y)$, $\boldsymbol{k}_3 = \boldsymbol{k}_z = (\kappa, 0)$ and replacing the subscripts 1 by t for a turbulent mode, 2 by s a streamer and 3 by z for the zonal flow. One further defines $k^2 = \kappa^2 + k_y^2$ that replaces k_1^2. In this case one finds how a particular zonal flow pattern with finite amplitude can destabilize a turbulent mode and a streamer pattern. One then obtains:

$$\partial_t \widehat{\phi}_t - \frac{k_y^2 - \kappa^2}{k^2}\kappa k_y \widehat{\phi}_s \widehat{\phi}_z + \gamma_t \widehat{\phi}_t = 0 \tag{B.3a}$$

$$\partial_t \widehat{\phi}_s + \kappa k_y \widehat{\phi}_t \widehat{\phi}_z^* + \gamma_s \widehat{\phi}_s = 0 \tag{B.3b}$$

where $\gamma_t = A_\phi(\boldsymbol{k}_t)$ and $\gamma_s = A_\phi(\boldsymbol{k}_t s)$. The determinant of the system (B.3) then yields (3b). The two roots of the latter are given by:

$$\Big(\gamma_2 + \gamma_2 \frac{\gamma_t + \gamma_s}{2}\Big)^2 = \Big(\frac{\gamma_t + \gamma_s}{2}\Big)^2 - \gamma_t\gamma_s - V_t k_y^2 \kappa^2 |\widehat{\phi}_z|^2 \tag{B.3c}$$

where $V_t = (k_y^2 - \kappa^2)/k^2$. The condition for instability is that $\gamma_t\gamma_s + V_t k_y^2 \kappa^2 |\widehat{\phi}_z|^2 \leq 0$ and a necessary condition is therefore that $V_t < 0$, hence $k_y^2 < \kappa^2$. Alternatively, the general system (B.2) can be simplified with the particular choice $\boldsymbol{k}_1 = \boldsymbol{k}_t = (\kappa, k_y)$, $\boldsymbol{k}_2 = \boldsymbol{k}_z = (\kappa, 0)$, $\boldsymbol{k}_3 = \boldsymbol{k}_s = (0, k_y)$ and replacing the subscripts 1 by t, 2 by z and 3 by s with a complex conjugate to account for the minus sign. In this case one finds how a particular streamer pattern with finite amplitude can destabilize a turbulent mode and a zonal flow pattern. One then obtains:

$$\partial_t \widehat{\phi}_t - \frac{k_y^2 - \kappa^2}{k^2} k_y \kappa \widehat{\phi}_z \widehat{\phi}_s + \gamma_t \widehat{\phi}_t = 0 \tag{B.4a}$$

$$\partial_t \widehat{\phi}_z - \kappa k_y \widehat{\phi}_z \widehat{\phi}_s^* + \gamma_z \widehat{\phi}_z = 0 \tag{B.4b}$$

where $\gamma_z = A_\phi(\boldsymbol{k}_z)$. The determinant of the system (B.4) then yields (3a). The two roots of the latter are given by:

$$\left(\gamma_1 + \gamma_1 \frac{\gamma_t + \gamma_z}{2}\right)^2 = \left(\frac{\gamma_t + \gamma_z}{2}\right)^2 - \gamma_t\gamma_z + V_t k_y^2 \kappa^2 |\widehat{\phi}_s|^2 \tag{B.4c}$$

The condition for instability is that $-\gamma_t\gamma_z + V_t k_y^2 \kappa^2 |\widehat{\phi}_z|^2 \geq 0$ and a necessary condition is therefore that $V_t > 0$, hence $k_y^2 > \kappa^2$.

Bibliography

[1] Nikolai A. Maximenko, Bohyun Bang, and Hideharu Sasaki. Observational evidence of alternating zonal jets in the world ocean. *Geophys. Res. Lett.*, 32(12):L12607–, 2005.

[2] Ashwin R Vasavada and Adam P Showman. Jovian atmospheric dynamics: an update after Galileo and Cassini. *Reports on Progress in Physics*, 68(8):1935, 2005.

[3] K. H. Burrell. Effects of E x B velocity shear and magnetic shear on turbulence and transport in magnetic confinement devices. *Physics of Plasmas (1994-present)*, 4(5):1499–1518, 1997.

[4] Akihide Fujisawa. A review of zonal flow experiments. *Nuclear Fusion*, 49(1):013001, 2009.

[5] K. H. Burrell. Role of sheared E x B flow in self-organized, improved confinement states in magnetized plasmas. *Physics of Plasmas*, 27(6):060501, 2020.

[6] Boris Galperin, Semion Sukoriansky, and Nadejda Dikovskaya. Zonostrophic turbulence. *Physica Scripta*, 2008(T132):014034, 2008.

[7] P H Diamond, S-I Itoh, K Itoh, and T S Hahm. Zonal flows in plasma - a review. *Plasma Physics and Controlled Fusion*, 47(5):R35, 2005.

[8] Jeffrey B. Parker and John A. Krommes. Zonal flow as pattern formation. *Physics of Plasmas (1994-present)*, 20(10):–, 2013.

[9] Akira Hasegawa and Kunioki Mima. Pseudo-three-dimensional turbulence in magnetized nonuniform plasma. *Physics of Fluids*, 21(1):87–92, 1978.

[10] Boris Galperin, Semion Sukoriansky, and Nadejda Dikovskaya. Geophysical flows with anisotropic turbulence and dispersive waves: flows with a β effect. *Ocean Dynamics*, 60(2):427–441, 2010.

[11] X. Garbet, L. Laurent, J.-P. Roubin, and A. Samain. A model for the turbulence in the scrape-off layer of tokamaks. *Nuclear Fusion*, 31(5):967, 1991.

[12] A. V. Nedospasov. The enhancement of edge turbulence in tokamaks by a limiter current. *Physics of Fluids B: Plasma Physics*, 5(9):3191–3194, 1993.

[13] Christiane Normand, Yves Pomeau, and Manuel G. Velarde. Convective instability: A physicist's approach. *Review of Modern Physics*, 49:581–624, Jul 1977.

[14] Ph. Ghendrih, Y. Sarazin, G. Attuel, S. Benkadda, P. Beyer, G. Falchetto, C. Figarella, X. Garbet, V. Grandgirard, and M. Ottaviani. Theoretical analysis of the influence of external biasing on long range turbulent transport in the scrape-off layer. *Nuclear Fusion*, 43(10):1013, 2003.

[15] F. Wilczynski, D. W. Hughes, S. Van Loo, W. Arter, and F. Militello. Stability of scrape-off layer plasma: A modified Rayleigh-Bénard problem. *Physics of Plasmas*, 26(2):022510, 2019.

[16] Y. Sarazin and Ph. Ghendrih. Intermittent particle transport in two-dimensional edge turbulence. *Physics of Plasmas*, 5(12):4214–4228, 1998.

[17] G. Dif-Pradalier, P. H. Diamond, V. Grandgirard, Y. Sarazin, J. Abiteboul, X. Garbet, Ph. Ghendrih, A. Strugarek, S. Ku, and C. S. Chang. On the validity of the local diffusive paradigm in turbulent plasma transport. *Phys. Rev. E*, 82(2):025401–, August 2010.

[18] G. Dif-Pradalier, G. Hornung, Ph. Ghendrih, Y. Sarazin, F. Clairet, L. Vermare, P. H. Diamond, J. Abiteboul, T. Cartier-Michaud, C. Ehrlacher, D. Estève, X. Garbet, V. Grandgirard, Ö. D. Gürcan, P. Hennequin, Y. Kosuga, G. Latu, P. Maget, P. Morel, C. Norscini, R. Sabot, and A. Storelli. Finding the Elusive $\mathbf{E} \times \mathbf{B}$ Staircase in Magnetized Plasmas. *Physics Review Letters*, 114:085004, Feb 2015.

[19] P. Ghendrih, Y. Asahi, E. Caschera, G. Dif-Pradalier, P. Donnel, X. Garbet, C. Gillot, V. Grandgirard, G. Latu, Y. Sarazin, S. Baschetti, H. Bufferand, T. Cartier-Michaud, G. Ciraolo, P. Tamain, R. Tatali, and E. Serre. Generation and dynamics of SOL corrugated profiles. *Journal of Physics: Conference Series*, 1125(1):012011, 2018.

[20] Claudia Norscini. *Self-organized turbulent transport in fusion plasmas*. PhD thesis, Université d'Aix Marseille, 2015.

[21] M. A. Mahdavi, R. Maingi, R. J. Groebner, A. W. Leonard, T. H. Osborne, and G. Porter. Physics of pedestal density profile formation and its impact on H-mode density limit in burning plasmas. *Physics of Plasmas*, 10(10):3984–3991, 2003.

[22] F. Wagner, G. Becker, K. Behringer, D. Campbell, A. Eberhagen, W. Engelhardt, G. Fussmann, O. Gehre, J. Gernhardt, G. v. Gierke, G. Haas, M. Huang, F. Karger, M. Keilhacker, O. Klüber, M. Kornherr, K. Lackner, G. Lisitano, G. G. Lister, H. M. Mayer, D. Meisel, E. R. Müller, H. Murmann, H. Niedermeyer, W. Poschenrieder, H. Rapp, H. Röhr, F. Schneider, G. Siller, E. Speth, A. Stäbler, K. H. Steuer, G. Venus, O. Vollmer, and Z. Yü. Regime of Improved Confinement and High Beta in Neutral-Beam-Heated Divertor Discharges of the ASDEX Tokamak. *Physical Review Letters*, 49:1408–1412, Nov 1982.

[23] T. Cartier-Michaud, P. Ghendrih, Y. Sarazin, J. Abiteboul, H. Bufferand, G. Dif-Pradalier, X. Garbet, V. Grandgirard, G. Latu, C. Norscini, C. Passeron, and P. Tamain. Projection on Proper elements for code control: Verification, numerical convergence, and reduced models. application to plasma turbulence simulations. *Physics of Plasmas*, 23(2), 2016.

[24] A. M. Dimits, G. Bateman, M. A. Beer, B. I. Cohen, W. Dorland, G. W. Hammett, C. Kim, J. E. Kinsey, M. Kotschenreuther, A. H. Kritz, L. L. Lao, J. Mandrekas, W. M. Nevins, S. E. Parker, A. J. Redd, D. E. Shumaker, R. Sydora, and J. Weiland. Comparisons and physics basis of tokamak transport models and turbulence simulations. *Physics of Plasmas (1994-present)*, 7(3):969–983, 2000.

[25] Plamen G. Ivanov, A. A. Schekochihin, W. Dorland, A. R. Field, and F. I. Parra. Zonally dominated dynamics and Dimits threshold in curvature-driven ITG turbulence. *Journal of Plasma Physics*, 86(5):855860502, 2020.

[26] Ph Ghendrih, C Norscini, F Hasenbeck, G Dif-Pradalier, J Abiteboul, T Cartier-Michaud, X Garbet, V Grandgirard, Y Marandet, Y Sarazin, P Tamain, and D Zarzoso. Thermodynamical and microscopic properties of turbulent transport in the edge plasma. *Journal of Physics: Conference Series*, 401(1):012007, 2012.

[27] Y. Sarazin, X. Garbet, Ph. Ghendrih, and S. Benkadda. Transport due to front propagation in tokamaks. *Physics of Plasmas (1994-present)*, 7(4):1085–1088, 2000.

[28] S. I. Krasheninnikov. On scrape off layer plasma transport. *Physics Letters A*, 283(5):368–370, 2001.

[29] S J Zweben, J R Myra, W M Davis, D A D'Ippolito, T K Gray, S M Kaye, B P LeBlanc, R J Maqueda, D A Russell, and D P Stotler and. Blob structure and motion in the edge and SOL of NSTX. *Plasma Physics and Controlled Fusion*, 58(4):044007, jan 2016.

[30] N. Fedorczak, A. Gallo, P. Tamain, H. Bufferand, G. Ciraolo, and Ph. Ghendrih. On the dynamics of blobs in scrape-off layer plasma: Model validation from two-dimensional simulations and experiments in tore supra. *Contributions to Plasma Physics*, 58(6-8):471–477, 2018.

[31] E Floriani, G Ciraolo, Ph Ghendrih, R Lima, and Y Sarazin. Self-regulation of turbulence bursts and transport barriers. *Plasma Physics and Controlled Fusion*, 55(9):095012, 2013.

[32] X. Garbet, O. Panico, R. Varennes, C. Gillot, G. Dif-Pradalier, Y. Sarazin, V. Grandgirard, P. Ghendrih, and L. Vermare. Wave trapping and e x b staircases. *Physics of Plasmas*, 28(4):042302, 2021.

[33] Philippe Ghendrih, Claudia Norscini, Thomas Cartier-Michaud, Guilhem Dif-Pradalier, Jérémie Abiteboul, Yue Dong, Xavier Garbet, Ozgür Gürcan, Pascale Hennequin, Virginie Grandgirard, Guillaume Latu, Pierre Morel, Yanick Sarazin, Alexandre Storelli, and Laure Vermare. Phase space structures in gyrokinetic simulations of fusion plasma turbulence. *The European Physical Journal D*, 68(10), 2014.

[34] Isabelle Daumont, Thierry Dauxois, and Michel Peyrard. Modulational instability: first step towards energy localization in nonlinear lattices. *Nonlinearity*, 10(3):617–630, may 1997.

[35] Z. Lin, T. S. Hahm, W. W. Lee, W. M. Tang, and P. H. Diamond. Effects of collisional zonal flow damping on turbulent transport. *Phys. Rev. Lett.*, 83:3645–3648, Nov 1999.

[36] Y. Sarazin. *Etude de la turbulence de bord dans les plasmas de tokamaks*. PhD thesis, 1997.

[37] M. G. Shats, H. Xia, and H. Punzmann. Spectral condensation of turbulence in plasmas and fluids and its role in low-to-high phase transitions in toroidal plasma. *Phys. Rev. E*, 71:046409, Apr 2005.

[38] P. H. Diamond, Y.-M. Liang, B. A. Carreras, and P. W. Terry. Self-regulating shear flow turbulence: A paradigm for the L to H transition. *Phys. Rev. Lett.*, 72:2565–2568, Apr 1994.

[39] K. Miki, P. H. Diamond, Ö. D. Gürcan, G. R. Tynan, T. Estrada, L. Schmitz, and G. S. Xu. Spatio-temporal evolution of the L $\rightarrow$ I $\rightarrow$ H transition. *Physics of Plasmas*, 19(9):092306,

2012.

[40] B. E. Launder and D. B. Spalding. The numerical computation of turbulent flows. *Computer Methods in Applied Mechanics and Engineering*, 3(2):269 – 289, 1974.

[41] S. Baschetti, H. Bufferand, G. Ciraolo, Ph. Ghendrih, E. Serre, P. Tamain, and the WEST Team. Self-consistent cross-field transport model for core and edge plasma transport. 61(10):106020, sep 2021.

[42] E Joffrin, C. D. Challis, G. D. Conway, X. Garbet, A. Gude, S. Günter, N. C. Hawkes, T. C. Hender, D. F. Howell, G. T. A Huysmans, E. Lazzaro, P. Maget, M. Marachek, A. G. Peeters, S. D. Pinches, S. E. Sharapov, and JET-EFDA contributors. Internal transport barrier triggering by rational magnetic flux surfaces in tokamaks. *Nuclear Fusion*, 43(10):1167–1174, sep 2003.

[43] J.W. Connor, T. Fukuda, X. Garbet, C. Gormezano, V. Mukhovatov, M. Wakatani, the ITB Database Group, the ITPA Topical Group on Transport, and Internal Barrier Physics. A review of internal transport barrier physics for steady-state operation of tokamaks. *Nuclear Fusion*, 44(4):R1, 2004.

[44] L. Chôné, P. Beyer, Y. Sarazin, G. Fuhr, C. Bourdelle, and S. Benkadda. L-H transition dynamics in fluid turbulence simulations with neoclassical force balance. *Physics of Plasmas*, 21(7):070702, 2014.

[45] A. H. Nielsen, G. S. Xu, J. Madsen, V. Naulin, Juul Rasmussen, and B. N. Wan. Simulation of transition dynamics to high confinement in fusion plasmas. *Physics Letters A*, 379(47):3097–3101, 2015.

[46] Davide Galassi, Guido Ciraolo, Patrick Tamain, Hugo Bufferand, Philippe Ghendrih, Nicolas Nace, and Eric Serre. Tokamak Edge Plasma Turbulence Interaction with Magnetic X-Point in 3D Global Simulations. *Fluids*, 4(1), 2019.

[47] E. Caschera, G. Dif-Pradalier, Ph. Ghendrih, V. Grandgirard, Y. Asahi, N. Bouzat, P. Donnel, X. Garbet, G. Latu, C. Passeron, and Y. Sarazin. Immersed boundary conditions in global, flux-driven, gyrokinetic simulations. 1125:012006, nov 2018.

[48] Elisabetta Caschera. *Global confinement properties of Tokamak plasmas in global, flux-driven, gyrokinetic simulations*. Theses, Aix-Marseille Université, Marseille, France, November 2019.

[49] Guilhem Dif-Pradalier, Philippe Ghendrih, Yanick Sarazin, Elisabetta Caschera, Frederic Clairet, Yann Camenen, Xavier Garbet, Virginie Grandgirard, Yann Munschy, Laure Vermare, and Fabien Widmer. Transport in fusion plasmas: Is the tail wagging the dog? sep 2021.

[50] T. Cartier-Michaud, P. Ghendrih, Y. Sarazin, G. Dif-Pradalier, T. Drouot, D. Estève, X. Garbet, V. Grandgirard, G. Latu, C. Norscini, and C. Passeron. Staircase temperature profiles and plasma transport self-organisation in a minimum kinetic model of turbulence based on the trapped ion mode instability. *Journal of Physics: Conference Series*, 561(1):012003, 2014.

[51] Akira Hasegawa and Masahiro Wakatani. Plasma edge turbulence. *Phys. Rev. Lett.*, 50:682–686, Feb 1983.